Electronic Supplementary Material (ESI) for Journal of Materials Chemistry A.

Supplementary Information

Facile synthesis of novel, known, and low-valent transition metal phosphates via reductive phosphatization

Niklas Stegmann,[a] Hilke Petersen,[a] Claudia Weidenthaler [a]
and Wolfgang Schmidt *[a]

Max-Planck-Institut für Kohlenforschung
Department of Heterogeneous Catalysis
Kaiser-Wilhelm-Platz 1, D-45470 Mülheim an der Ruhr, Germany
E-mail: schmidt@mpi-muelheim.mpg.de

Characterization

Powder X-ray diffraction (XRD)

XRD patterns were measured either on a Stoe STADI P θ/2θ diffractometer (Bragg-Brentano geometry) or a Stoe STADI P transmission diffractometer (Debye-Scherrer geometry) using 0.5 mm borosilicate capillaries for transmission measurements. The transmission diffractometer was equipped with a primary germanium monochromator and a position-sensitive detector provided by Stoe, the reflection instrument was equipped with an energy-dispersive PIN diode detector. Both instruments were operated with Cu K_α radiation.

Raman spectroscopy

The Raman data were recorded on an InVia spectroscope (Renishaw Ltd, UK) with an excitation wavelength of 785 nm; the laser power was tuned to 30mW. A 1200 grating/mm grid assured a spectra resolution of 1 cm^{-1}. All spectra were collected with 10 s per step and three repetitions.

Thermogravimetric analysis and mass spectrometry

TG/DSC measurements have been performed with a Netzsch STA 449 DSC/TG instrument attached to a Netzsch Aeolos quadrupole mass spectrometer. Measurements have been performed under argon atmosphere using a heating rate of 10°C/min.

X-ray photoelectron spectroscopy

XPS measurements were performed with a spectrometer from SPECS GmbH equipped with a PHOIBOS 150 1D-DLD hemispherical energy analyser. The monochromatized Al K_α X-ray source (E=1486.6 eV) was operated at 15 kV and 200 W. For measuring high-resolution scans, the pass energy was set to 20 eV. The medium area mode was used as lens mode. The base pressure during the experiment in the analysis chamber was $5 \cdot 10^{-10}$ mbar. To account for charging effects, all spectra are referenced to the C 1s binding energy of 284.5 eV.

MAS NMR spectroscopy

^{31}P MAS NMR spectra were recorded on a Bruker Avance III HD 500WB spectrometer using a double-bearing MAS probe (DVT BL4) at a resonance frequency of 202.5 MHz. The spectra were measured by applying single π/2-pulses (3.0 μs) with a recycle delay of 600 s (4 or 8 scans) at several spinning rates between 3 and 12°kHz. High-power proton decoupling (spinal64) was applied. The chemical shifts are given with respect to 85% aqueous H_3PO_4 using solid $NH_4H_2PO_4$ as secondary reference ($\delta = 0.81$ ppm).

Mössbauer spectroscopy

Mössbauer spectra were recorded on a spectrometer with alternating constant acceleration of the γ-source. The minimum experimental line width of the instrument was 0.24 mm/s (full width at half-height). The sample temperature was maintained constant in an Oxford Instruments Variox cryostat, whereas the ^{57}Co/Rh source (0.9 GBq) was kept at room temperature. The detector was a Si-Drift diode (150 mm^2 SDD CUBE) of an AXAS-M1 system from Ketek GmbH. The spectrometer was calibrated by recording the Mössbauer spectrum of 25 µm alpha-Fe foil at room temperature. As the center of the six-line pattern was taken as zero velocity, isomer shifts are quoted relative to iron metal at 300K. The zero-field spectra were simulated with Lorentzians by using the program *mf.SL* (by EB).

Scanning electron microscopy (SEM)

SEM imaging were performed with a TM3030 PLUS table-top electron microscope from Hitachi operated at 15 kV. Electron detection via BSE or SE detector or both detectors combined.

Syntheses

The general synthetic procedure of TMPs via the molten salt method is illustrated in **Figure S1**. In a typical preparation, metal oxide powder (TiO_2, V_2O_5, Cr_2O_3, MnO_2, Fe_2O_3) is mixed with a surplus of ammonium hypophosphite ($NH_4H_2PO_2$) with weight ratios up to 1/10 and heated for 2 h in a tube furnace under argon flow. Finally, the sample is cooled down and washed with de-ionized water until pH 6 is achieved for removing excess phosphates from the crystalline material.

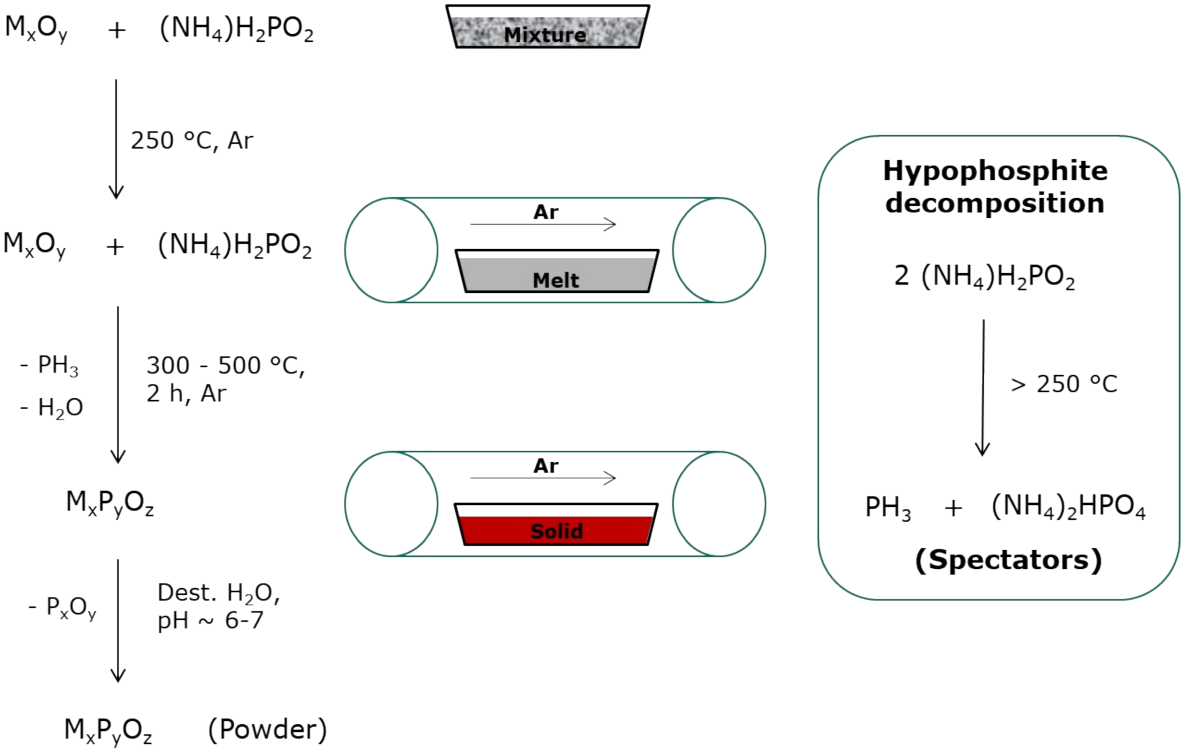

Figure S1. Illustration of the general synthesis procedure for the preparation of TMPs by the molten salt method, starting from a solid mixture of ammonium hypophosphite and metal oxide.

Check of PH_3 as spectator species

Ammonium hypophosphite was decomposed at 500°C to release phosphane gas (PH_3). The formed PH_3 then was passed over TiO_2 (P25) in a continuous flow reactor under inert gas conditions at that temperature. Subsequently, the metal oxide powder was characterized via XRD which showed that no changes in crystallinity and phase composition of the precursor occurred. Thus, PH_3 does not react with the titanium oxide under these reaction conditions.

Synthesis of Ti(III)p at 300 °C

The synthesis of Ti(III)p was performed from a dry mixture of TiO_2 (P 25, Degussa, phase mixture of anatase and rutile, ≥ 99.5%) and $NH_4(H_2PO_2)$ (Fluka, ≥ 97.0%) with a weight ratio of 1/10. The synthesis was tested for batches in a range between 1 g and 10 g without any technical complications or deviations of the product crystallinity and purity. The mixture was filled in a ceramic crucible and heated in a tube furnace at 300 °C for 2 h under Ar flow (100 mL/min). A heating ramp of 10 °C/min was used up to 250 °C which then was decreased to 2 °C/min up to 300 °C. Finally, the sample was cooled down and washed with de-ionized water until pH 6 was achieved in the effluent. The powdery product was dried in air at 80 °C.

The synthesis of Ti(III)p is accompanied by several temperature depending events which are illustrated in **Figure S2**.

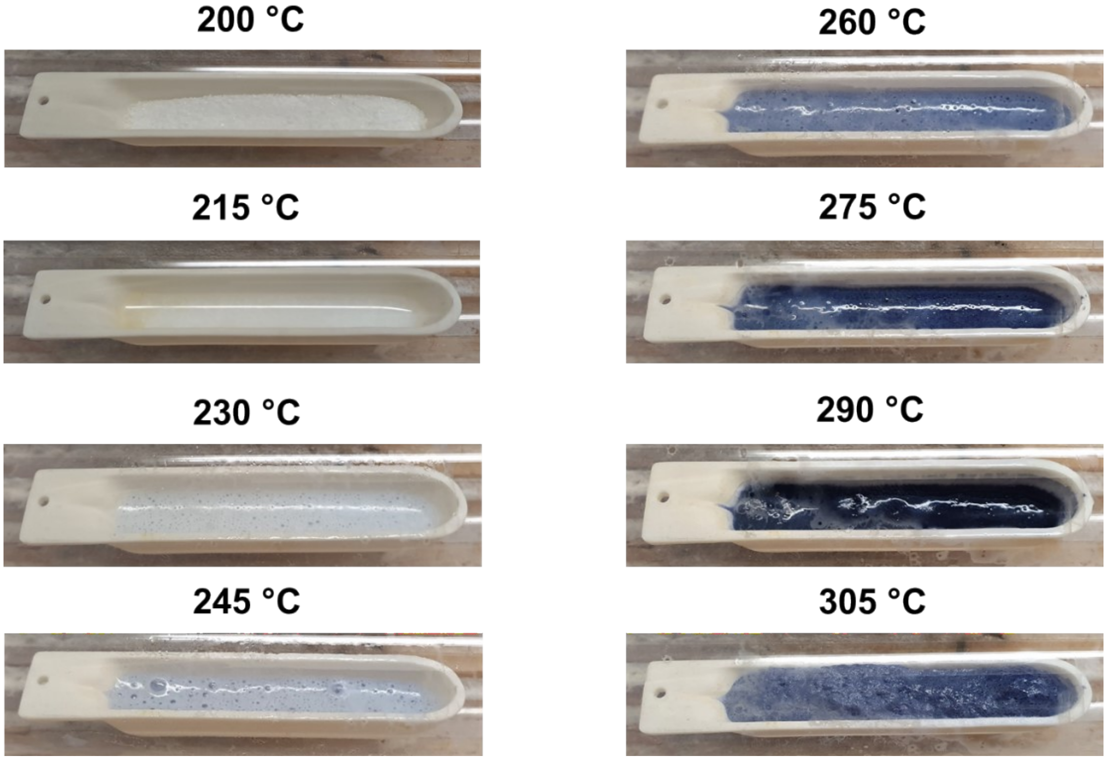

Figure S2. Photos taken during the preparation of Ti(III)p within a tube furnace at increasing temperatures**.**

Up to 200 °C the precursor mixture keeps a powdery form before ammonium hypophosphite starts to melt at 215°C (**Figure S2**). Partial thermal decomposition of the ammonium hypophosphite into phosphane and ammonium phosphate starts at temperatures above 230°C. Above 245°C the hypophosphite starts to react with titanium oxide as indicated by a deep purple coloration of the melt which is characteristic for the formation of titanium(III) species. Finally, the melt solidifies after the whole ammonium hypophosphite has reacted or decomposed.

Safety note: The thermal decomposition of ammonium hypophosphite causes the formation of gaseous phosphane (PH_3, CAS: 7803-51-2) which is known as a strong respiratory poison. Therefore, the preparation of TMPs by the presented molten salt method has to be implemented exclusively in closed systems under continuous inert gas flow.

Figure S3 shows the XRD pattern of Ti(III)p.

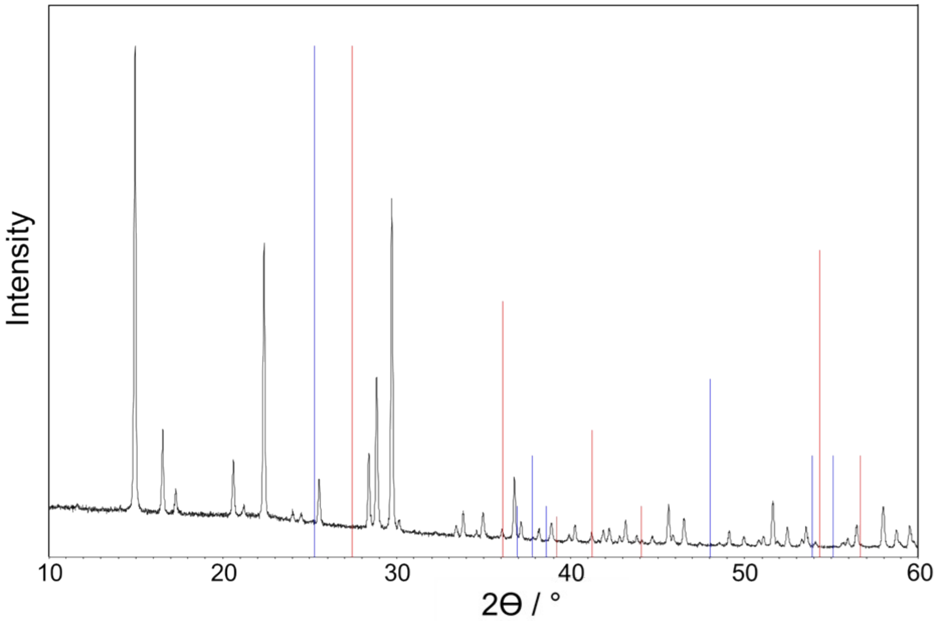

Figure S3. XRD pattern of Ti(III)p synthesized via reductive phosphatization of TiO2 (P25) in a melt of ammonium hypophosphite. Lines indicate the reflections of rutile (🟥) (PDF 00-021-1276) and anatase (🟦) (PDF 00-21-1272) phases of the TiO2 (P25) precursor.

Synthesis of Ti(IV)p at 500 °C

Ti(III)p obtained via the synthetic procedure described above was filled in a ceramic crucible and thermally treated at 500 °C under Ar flow (100 mL/min) for 4 h using a heating rate of 10 °C/min. Finally, the resulting white-yellowish powder was washed with de-ionized water and dried in air at 80 °C for 12 h. The phase transformation was tested for batches ranging from 100 mg to 1 g without any deviations of the product crystallinity and purity. **Figure S6** shows the XRD pattern of Ti(IV)p.

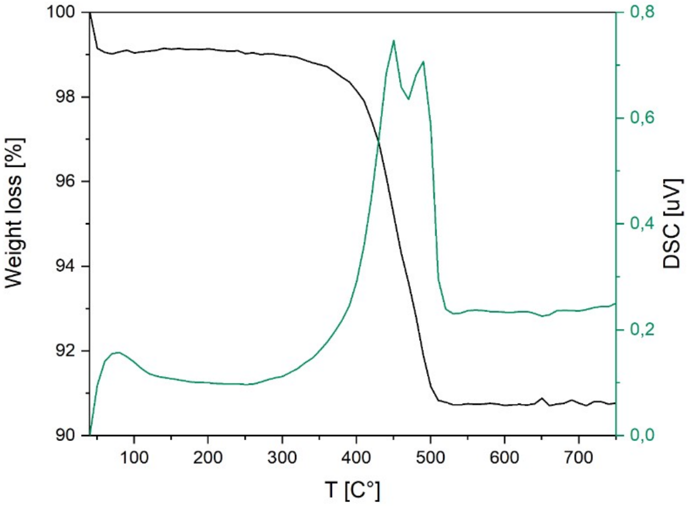

Figure S4. TG/DSC curves of the Ti(III)p → Ti(IV)p phase transformation.

TG/DSC performed on Ti(III)p under Ar atmosphere with a heating rate of 10 °C/min reveals a single step mass loss between 300 °C and 500 °C. The mass loss of 8wt% is accompanied by two endothermic signals (**Figure S4**) indicating the release of ammonia, hydrogen and water during the phase transformation (**Figure S5**). No additional gas species were observed in the experiments. Due to the high thermal stability of Ti(IV)p, no further transformations occur. The thermal decomposition of the ammonium cation causes the release of ammonia, while the protons are reduced to hydrogen during the oxidation of Ti(III) to Ti(IV) as illustrated in **Figure S5**. Release of H_2O is assumed to originate from condensation reactions of terminal phosphate groups on the surface of Ti(III)p precursor particles.

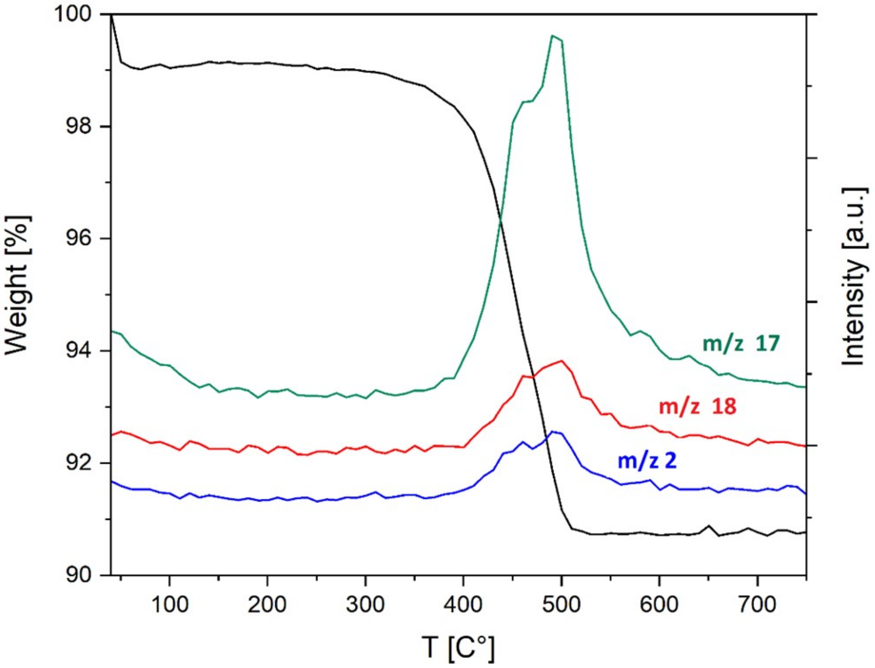

Figure S5. TG curve of Ti(III)p → Ti(IV)p phase transformation and associated mass signals of hydrogen (m/z 2), ammonia (m/z 17) and water (m/z 17, 18). The mass signals have been recorded from mass spectra of the exhaust gas of the TG/DSC instrument.

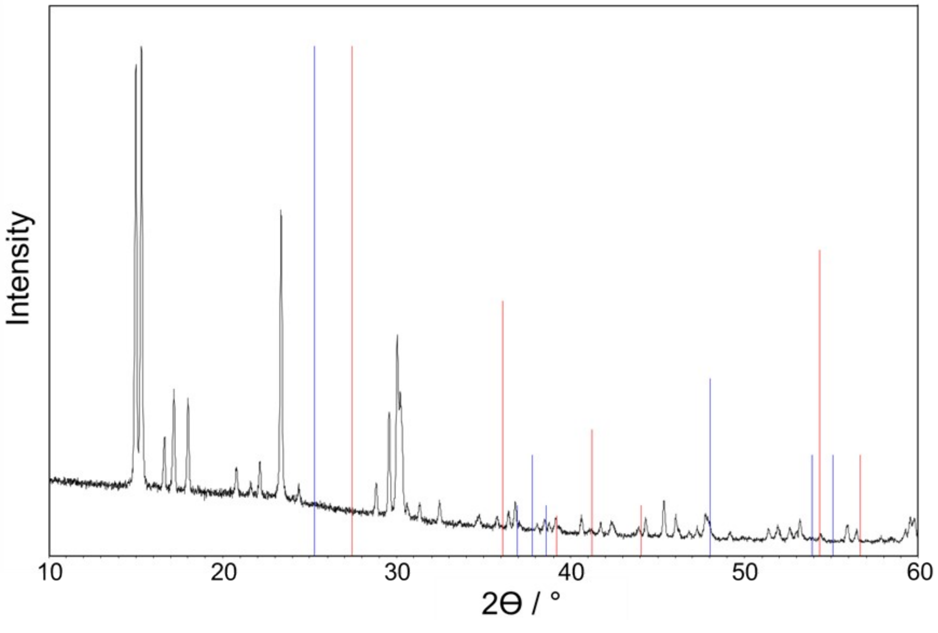

Figure S6. XRD pattern of Ti(IV)p synthesized by thermal treatment of Ti(III)p. Lines indicate the reflections of rutile (▬) (PDF 00-021-1276) and anatase (▬) (PDF 00-21-1272) phases of the TiO_2 (P25) precursor.

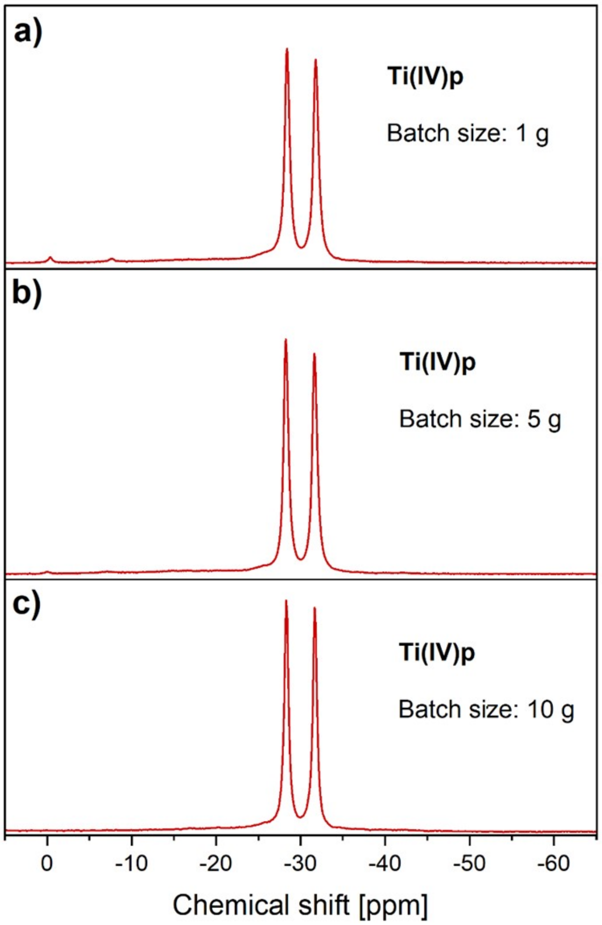

Figure S7. ^{31}P MAS NMR spectra of Ti(IV)p prepared via phase transformation from the Ti(III)p precursor phase. The Ti(III)p samples were prepared at different batches of 1 g, 5 g and 10 g.

Figure S7 shows ^{31}P MAS NMR spectra of three Ti(IV)p samples, which were prepared via phase transformation from the presented Ti(III)p precursor phase. The Ti(III)p precursor material was synthesized in different batches of 1 g, 5 g and 10 g (**Figure S7 a-c**). The signals around -30 ppm can be attributed to the pyrophosphate units of the crystalline Ti(IV)p samples. Spectra **a)** and **b)** show two small signals between 0 and -10 ppm which are characteristic for free ortho- and pyrophosphates which are not part of the crystal structure.[1] The ^{31}P MAS NMR spectra of Ti(IV)p show no additional phases and low amounts of amorphous parts, which indicates also a good purity of the Ti(III)p precursor material. Upscaling without losses in crystallinity and a high purity are features of the presented molten salt method.

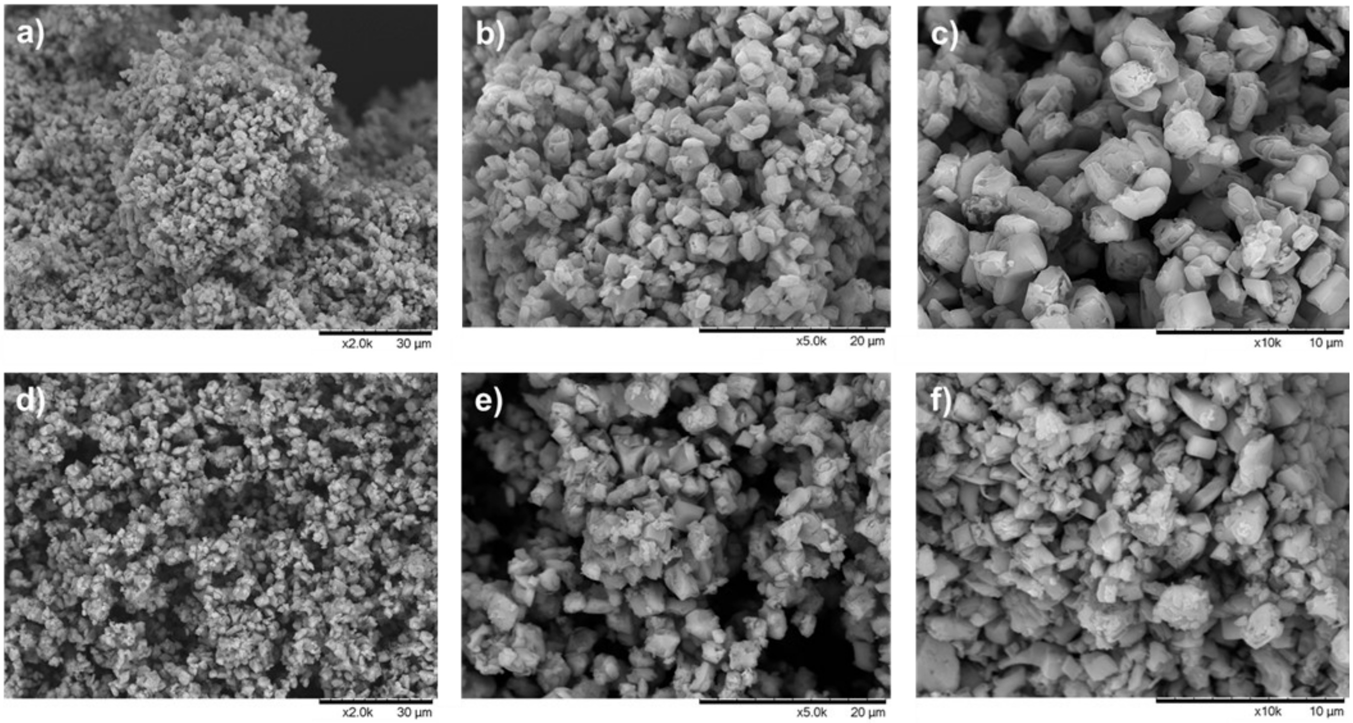

Figure S8. SEM images of a-c) Ti(III)p and d-f) Ti(IV)p synthesized via reductive phosphatization.

Synthesis of $Ti(PO_3)_3$ at 500 °C

The procedure used for the synthesis of $Ti(PO_3)_3$ is similar to that described for Ti(III)P with a difference in heating rate and temperature. A mixture of TiO_2 (P 25, Degussa) and $NH_4(H_2PO_2)$ (Fluka, ≥ 97.0%) with a weight ratio of 1/10 was filled in a ceramic crucible and heated in a tube furnace at 500 °C for 2 h under Ar flow (100 mL/min) using a heating rate of 10 °C/min. Finally, the sample was cooled down and washed with de-ionized water until pH 6 was achieved. The powdery product was dried at 80 °C in air. The synthesis was tested for batches ranging from 1 g to 5 g without any technical complications or deviations of the product crystallinity and purity. **Figure S9** shows the XRD pattern of $Ti(PO_3)_3$ and **Figure S10** shows SEM images of $Ti(PO_3)_3$.

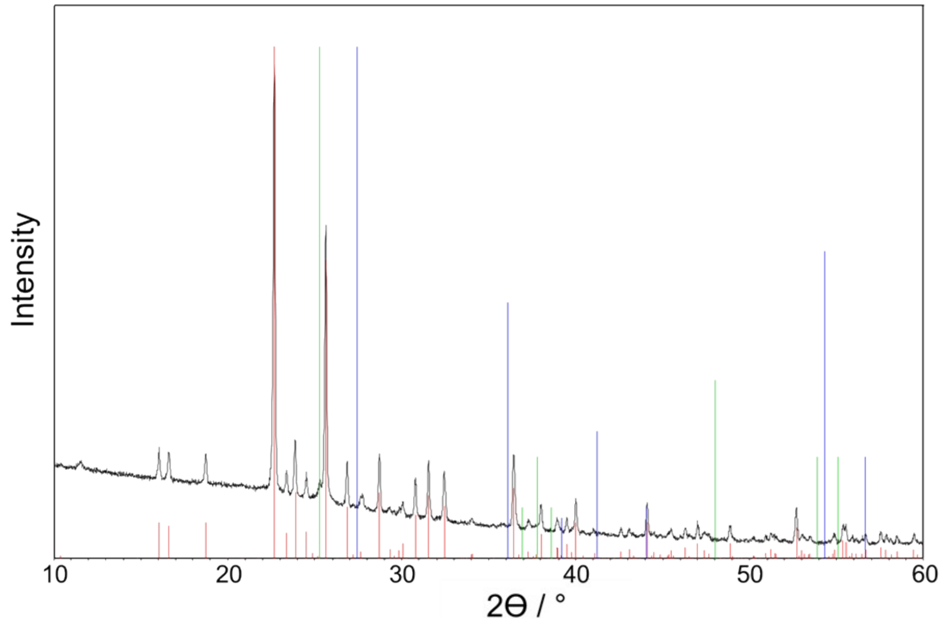

Figure S9. XRD pattern of $Ti(PO_3)_3$ synthesized via reductive phosphatization of TiO_2 (P25) in a melt of ammonium hypophosphite. Lines indicate the reflections of $Ti(PO_3)_3$ (—) (PDF 01-082-1178) as well as rutile (—) (PDF 00-021-1276) and anatase (—) (PDF 00-21-1272) phases of the TiO_2 (P25) precursor.

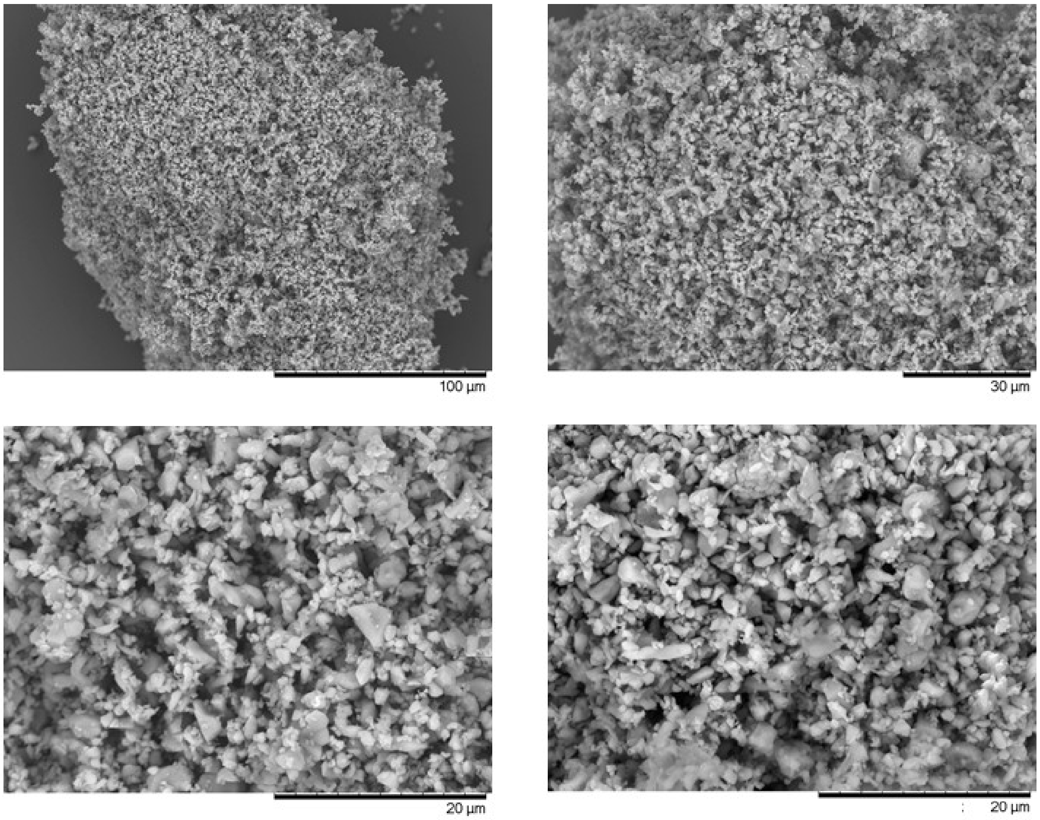

Figure S10. SEM images at different magnification of $Ti(PO_3)_3$ synthesized via reductive phosphatization of TiO_2 (P25) in a melt of ammonium hypophosphite.

Synthesis of $V(PO_3)_3$ at 300 °C

The synthesis of $V(PO_3)_3$ was performed from a mixture of 0.2 g V_2O_5 (Merck, ≥ 99%) and 2 g $NH_4(H_2PO_2)$ (Fluka, ≥ 97.0%) . The mixture was filled in a ceramic crucible and heated in a tube furnace at 300 °C for 2 h under Ar flow (100 mL/min). A heating ramp of 10 °C/min was used up to 250 °C which then was decreased to 2 °C/min up to 300 °C. Finally, the sample was cooled down and washed with de-ionized water until pH 6 was achieved. An additional washing step with ethanol was performed to avoid partial dissolution of the product by residual washing water during the drying process. The powdery product was dried in air at 80 °C.

Synthesis of $V(PO_3)_3$ at 500 °C

The procedure used for the synthesis of $V(PO_3)_3$ at 500°C is similar to those described above for 300 °C. The synthesis was performed from a mixture of 1 g V_2O_5 (Merck, ≥ 99%) and 10 g $NH_4(H_2PO_2)$ (Fluka, ≥ 97.0%). The mixture was filled in a ceramic crucible and heated in a tube furnace at 500 °C for 10 h under Ar flow (100 mL/min). A heating ramp of 10 °C/min was used up to 250 °C which then was decreased to 2 °C/min up to 500 °C Finally, the sample was cooled down and washed with de-ionized water until pH 6 was achieved in the effluent. An additional washing step with ethanol was carried out to avoid partial dissolution of the product by residual washing water during the drying process. The powdery product was dried in air at 80 °C. **Figure S11** shows the XRD pattern of $V(PO_3)_3$ and **Figure S12** shows SEM images of $V(PO_3)_{3.}$

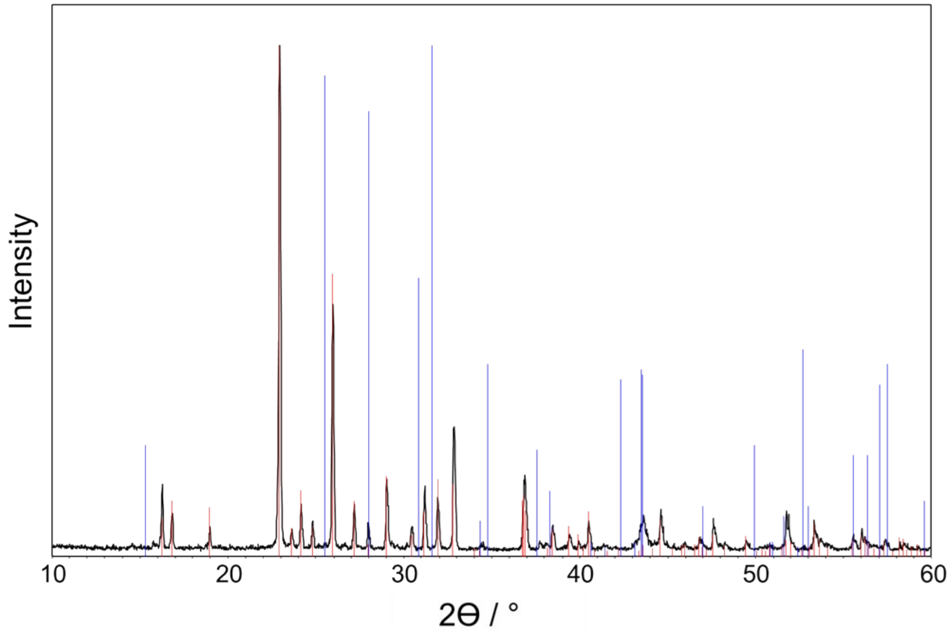

Figure S11. XRD pattern of $V(PO_3)_3$ synthesized via reductive phosphatization of V_2O_3 in a melt of ammonium hypophosphite. Lines indicate the reflections of $V(PO_3)_3$ (🟥) (PDF 01-072-2445) and V_2O_3 (🟦) (PDF 00-054-0513) precursor.

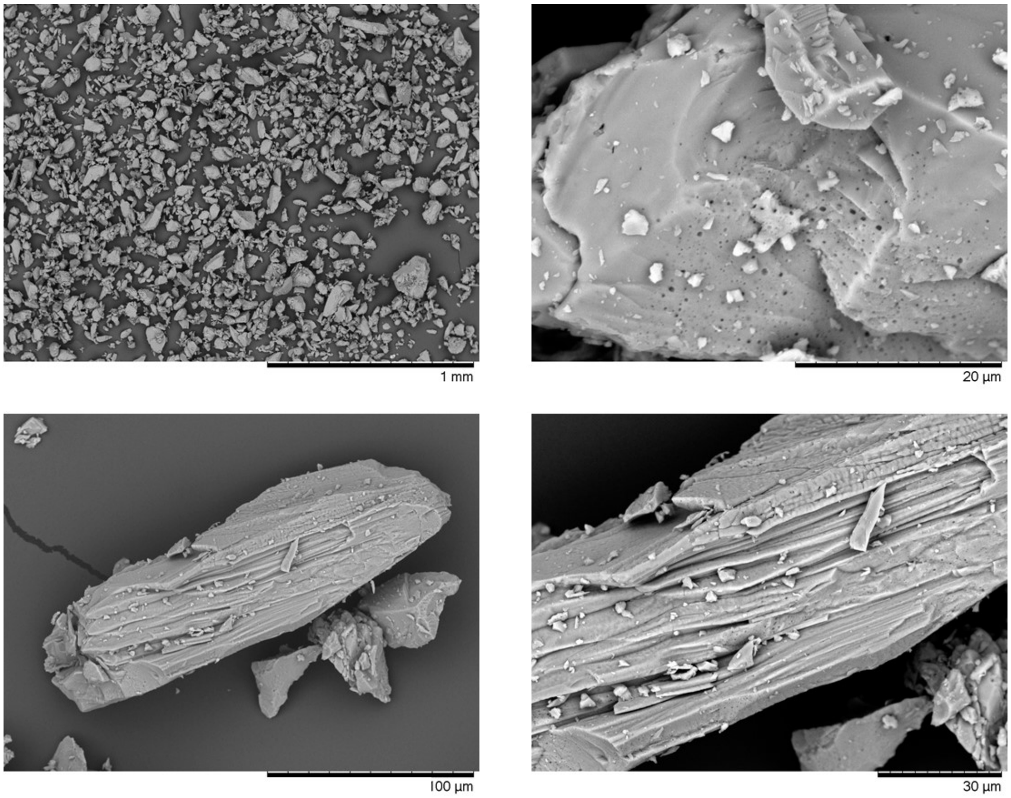

Figure S12. SEM images at different magnification of $V(PO_3)_3$ synthesized via reductive phosphatization of V_2O_3 in a melt of ammonium hypophosphite.

Synthesis of $Cr(NH_4)HP_3O_{10}$ at 300 °C

The synthesis of $Cr(NH_4)HP_3O_{10}$ was performed from a mixture of 0.5 g Cr_2O_3 (Merck, ≥ 98%) and 5 g $NH_4(H_2PO_2)$ (Fluka, ≥ 97.0%). The mixture was filled in a ceramic crucible and heated in a tube furnace at 300 °C for 10 h under Ar flow (100 mL/min). A heating ramp of 10 °C/min was used up to 250 °C which then was decreased to 2 °C/min up to 300 °C. Finally, the sample was cooled down and washed with de-ionized water until pH 6 was achieved in the effluent. An additional washing step with ethanol was carried out to avoid partial dissolution of the product by residual washing water during the drying process. The powdery product was dried at 80 °C in a ventilation oven over night and used for analysis. **Figure S13** shows the XRD pattern of $Cr(NH_4)HP_3O_{10}$.

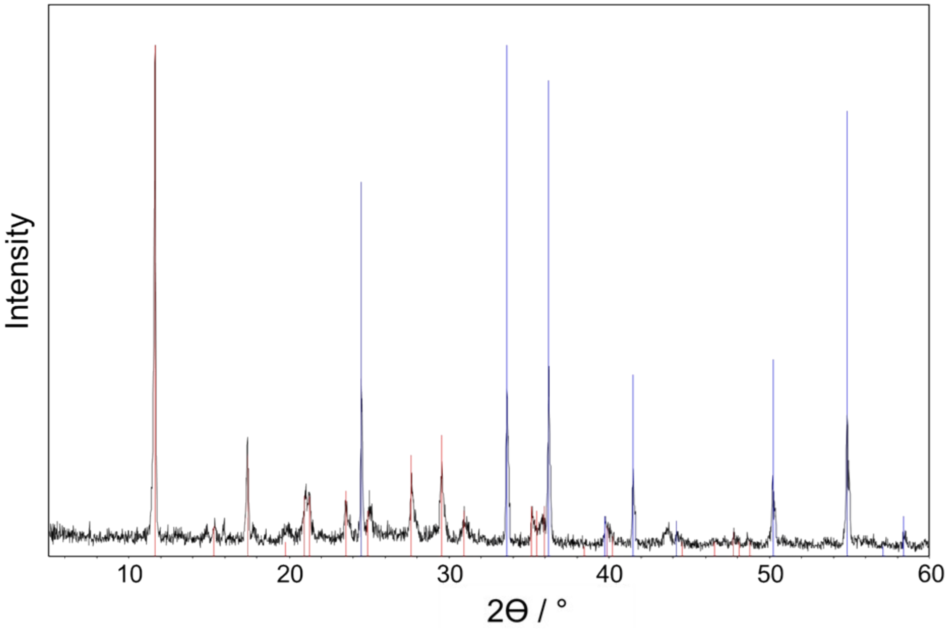

Figure S13. XRD pattern of $Cr(NH_4)HP_3O_{10}$ synthesized by the conversion of Cr_2O_3 in a melt of ammonium hypophosphite at 300 °C and additional reflexes belonging to the Cr_2O_3 precursor phase. Lines indicate the reflections of $Cr(NH_4)HP_3O_{10}$ (🟥) (PDF 00-038-0312) and Cr_2O_3 (🟦) (PDF 00-038-1479) precursor.

Synthesis of $Cr_2(P_6O_{18})$ at 500 °C

The synthesis of $Cr_2(P_6O_{18})$ was performed from a mixture of 0.2 g Cr_2O_3 (Merck, ≥ 98%) and 2 g $NH_4(H_2PO_2)$ (Fluka, ≥ 97.0%). The mixture was filled in a ceramic crucible and heated in a tube furnace at 500 °C for 4 h under Ar flow (100 mL/min) with a heating ramp of of 5 °C/min. Finally, the sample was cooled down and washed with de-ionized water until pH 6 was achieved in the effluent. An additional washing step with ethanol was carried out to avoid partial dissolution of the product by residual washing water during the drying process. The powdery product was dried at 80 °C in a ventilation oven over night and used for analysis. **Figure S14** shows the XRD pattern of $Cr_2(P_6O_{18})$.

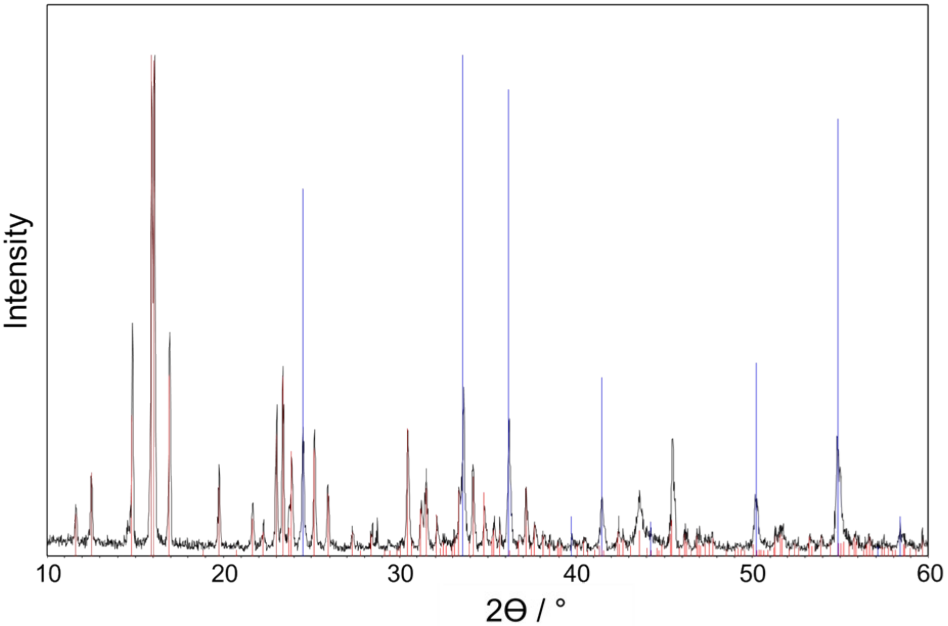

Figure S14. XRD pattern of $Cr_2(P_6O_{18})$ synthesized by the conversion of Cr_2O_3 in a melt of ammonium hypophosphite at 500 °C. Lines indicate the reflections of $Cr_2(P_6O_{18})$ (🟥) (PDF 01-070-0465) and Cr_2O_3 (🟦) (PDF 00-038-1479) precursor.

Synthesis of $Mn_2(P_4O_{12})$ at 500 °C

The synthesis of $Mn_2(P_4O_{12})$ was performed from a mixture of 0.2 g MnO_2 (Merck, ≥ 99.0%) and 1 g $NH_4(H_2PO_2)$ (Fluka, ≥ 97.0%). The mixture was filled in a ceramic crucible and heated in a tube furnace at 500 °C for 4 h under Ar flow (100 mL/min) with a heating ramp of of 10 °C/min. Finally, the sample was cooled down and washed with de-ionized water until pH 6 was achieved in the effluent. The powdery product was dried in air at 80 °C. **Figure S15** shows the XRD pattern of $Mn_2(P_4O_{12})$.

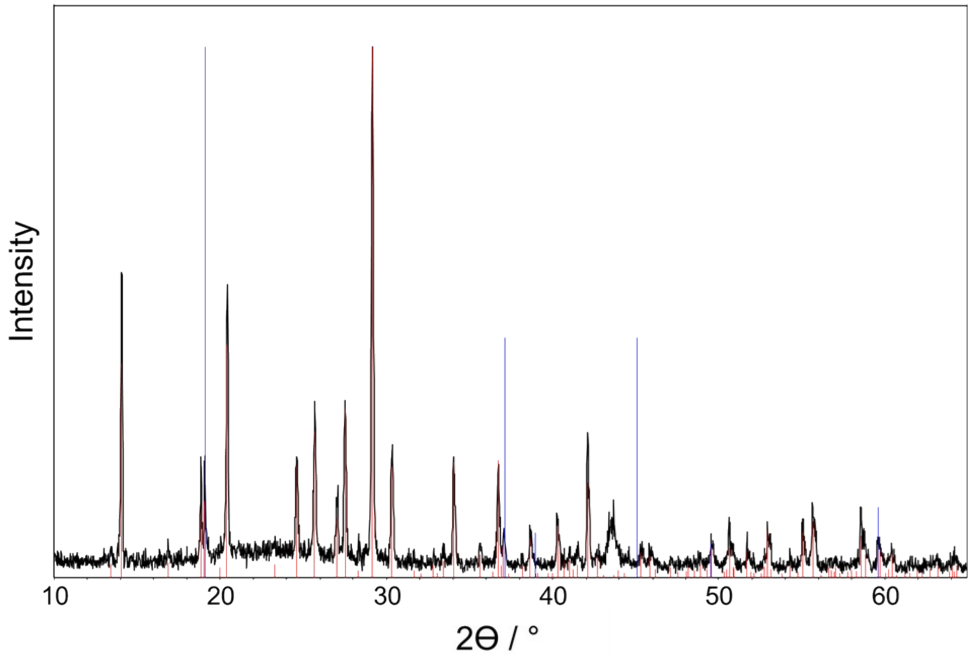

Figure S15. XRD pattern of $Mn_2(P_4O_{12})$ synthesized by the conversion of MnO_2 in a melt of ammonium hypophosphite at 500 °C. Lines indicate the reflections of $Mn_2(P_4O_{12})$ (—) (PDF 01-071-3438) and MnO_2(—) (PDF 00-044-0992) precursor.

Synthesis of Fe(II)p at 300 °C

The synthesis of the novel Fe(II)p compound was performed from a mixture of 0.5 g Fe_2O_3 (Riedel-de-Haen, ≥ 97%) and 5 g $NH_4(H_2PO_2)$ (Fluka, ≥ 97%). The mixture was filled in a ceramic crucible and heated in a tube furnace at 300 °C for 10 h under Ar flow (100 mL/min). A heating ramp of 10 °C/min was used up to 250 °C which was then decreased to 2 °C/min up to 300 °C. Finally, the sample was cooled down and washed with de-ionized water until pH 6 was achieved in the effluent. The powdery product was dried in air at 80 °C over night.

Figure S16 shows the XRD pattern of the novel iron(II) phosphate phase (Fe(II)p). **Figure S18** shows SEM images of Fe(II)p.

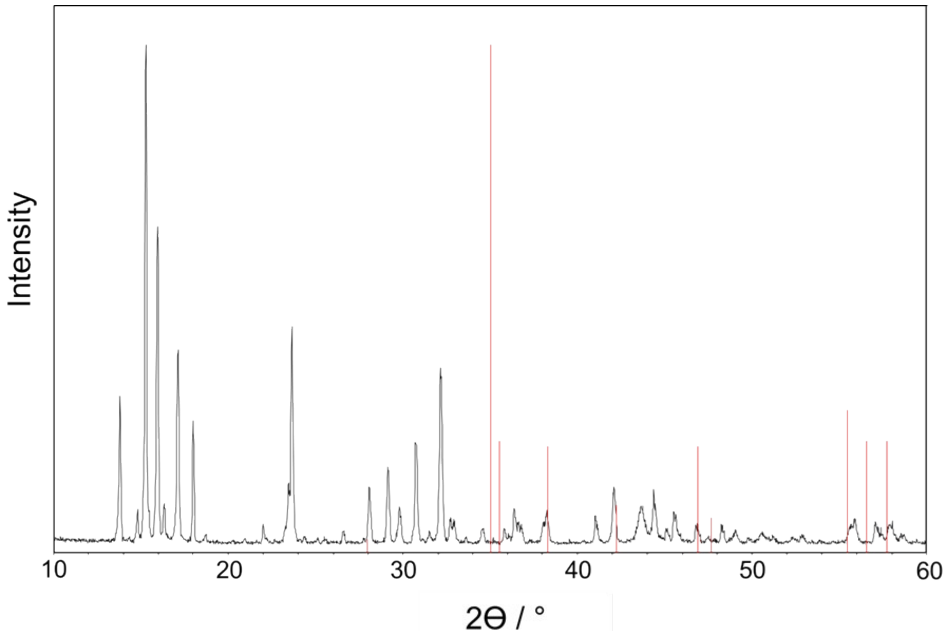

Figure S16. XRD pattern of Fe(II)p synthesized by the conversion of Fe_2O_3 in a melt of ammonium hypophosphite at 300 °C. Lines indicate the reflections of Fe_2O_3 (—) (PDF 00-056-1302) precursor.

Figure S17 shows the ^{57}Fe Mössbauer spectrum of Fe(II)p. Two different Mössbauer signals with isomer shifts in a range expected for Fe(II) high spin species are illustrated.[2] While the quadrupole splitting of first component (green line) is similar to that observed in $LiFePO_4$, the smaller quadrupole splitting of the second component (blue line) is quite small for Fe(II) high spin species. The sharp resonance signals of the spectrum indicate that the sample contains no significant amorphous parts of iron phosphate.

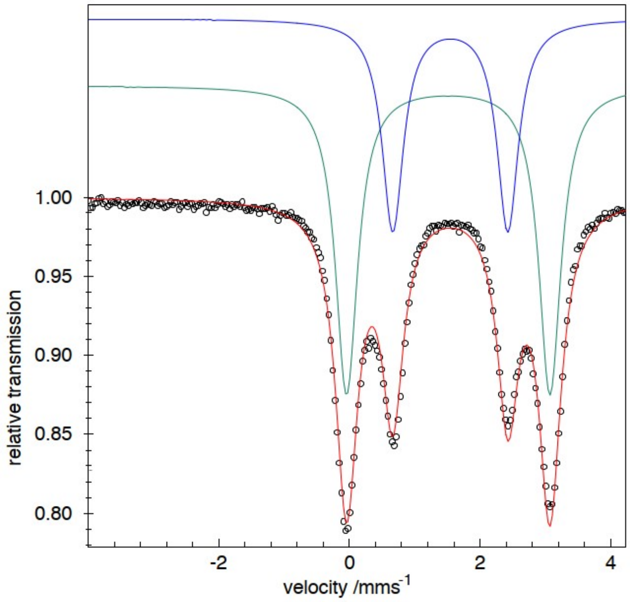

Figure S17. ^{57}Fe Mössbauer spectrum of Fe(II)p recorded at 80 K showing two Mössbauer sites with isomer shifts characteristic for Fe(II) species.

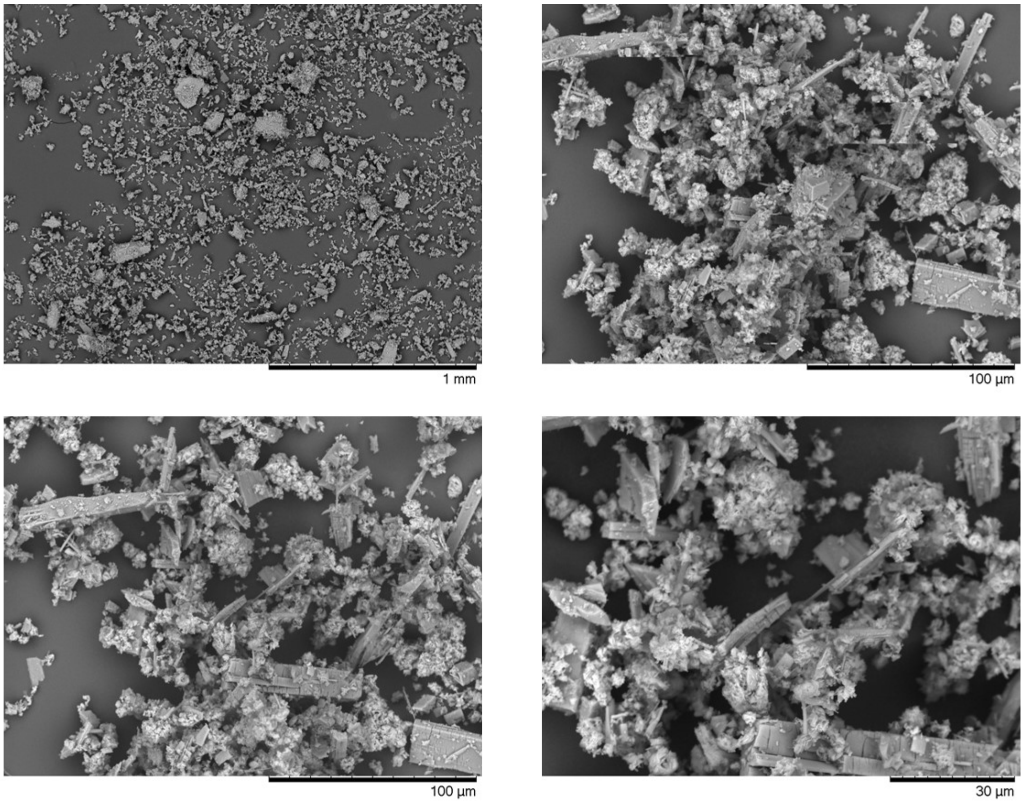

Figure S18. SEM images at different magnification of Fe(II)p synthesized by the conversion of Fe_2O_3 in a melt of ammonium hypophosphite at 300 °C.

Synthesis of $Fe_2(P_4O_{12})$ at 500 °C

The synthesis of $Fe_2(P_4O_{12})$ was performed from a mixture of 0.2 g Fe_2O_3 (Riedel-de-Haen, ≥ 97%) and 2 g $NH_4(H_2PO_2)$ (Fluka, ≥ 97%). The mixture was filled in a ceramic crucible and heated in a tube furnace at 500 °C for 10 h under Ar flow (100 mL/min) with a heating ramp of of 10 °C/min. Finally, the sample was cooled down and washed with de-ionized water until pH 6 was achieved in the effluent. The powdery product was dried in air at 80 °C over night. **Figure S19** shows the XRD pattern of $Fe_2(P_4O_{12})$.

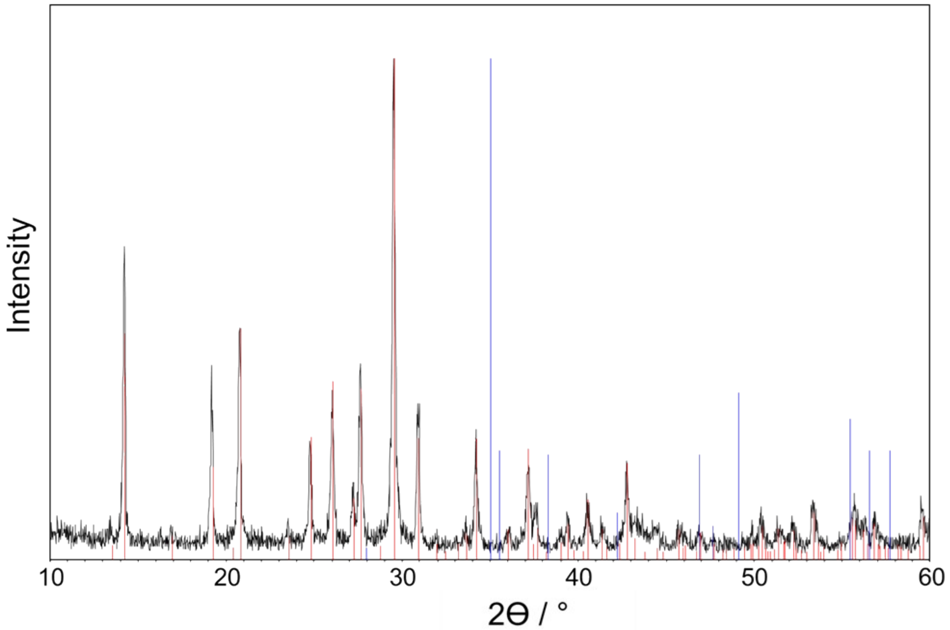

Figure S19. XRD pattern of $Fe_2(P_4O_{12})$ synthesized by the conversion of Fe_2O_3 in a melt of ammonium hypophosphite at 500 °C. Lines indicate the reflections of $Fe_2(P_4O_{12})$ (🟥) (PDF 00-056-1302) and Fe_2O_3 (🟦) (PDF 00-056-1302) precursor.

References

1. Hayashi, S. and K. Hayamizu, *High-Resolution Solid-State 31P NMR of Alkali Phosphates.* Bull. Chem. Soc. Jpn, 1989. **62**: p. 3061-3068.
2. Gütlich, P. and C. Schröder, *Mössbauer Spectroscopy.* Bunsen-Magazin, 2010. **12**(1): p. 4-23.